



Mannose-based surfactant as biofunctional nanoemulsion stabilizer

Pablo Argudo, Lea Spitzer, Emmanuel Ibarboure, François Jerome, Henri Cramail, Sébastien Lecommandoux

► To cite this version:

Pablo Argudo, Lea Spitzer, Emmanuel Ibarboure, François Jerome, Henri Cramail, et al.. Mannose-based surfactant as biofunctional nanoemulsion stabilizer. *Colloids and Surfaces B: Biointerfaces*, 2022, 220, pp.112877. 10.1016/j.colsurfb.2022.112877 . hal-03844794

HAL Id: hal-03844794

<https://hal.science/hal-03844794>

Submitted on 9 Nov 2022

HAL is a multi-disciplinary open access archive for the deposit and dissemination of scientific research documents, whether they are published or not. The documents may come from teaching and research institutions in France or abroad, or from public or private research centers.

L'archive ouverte pluridisciplinaire **HAL**, est destinée au dépôt et à la diffusion de documents scientifiques de niveau recherche, publiés ou non, émanant des établissements d'enseignement et de recherche français ou étrangers, des laboratoires publics ou privés.

Mannose-based surfactant as biofunctional nanoemulsion stabilizer

Pablo G. Argudo,^{1,‡,} Lea Spitzer,^{1,2,‡} Emmanuel Ibarboure,¹ François Jerome,² Henri Cramail,¹
Sébastien Lecommandoux,^{1,*}*

¹Univ. Bordeaux, CNRS, Bordeaux INP, LCPO, 16 Avenue Pey-Berland, 33600 Pessac, France

²Institut de Chimie des Milieux et Matériaux de Poitiers, CNRS-Université Poitiers, ENSIP, 1 rue
Marcel Doré, 86073 Poitiers, France

Abstract

The development and implementation of new amphiphiles based on natural resources rather than petrochemical precursors is an essential requirement due to their feedstock depletion and adverse environmental impacts. In addition, the use of bio-based surfactants can provide unique characteristics and improve the properties and versatility of the colloidal systems in which they are applied, such as emulsions. Here, the emulsification properties of a synthesized biocompatible mannose-based surfactant were investigated. Its behavior was evaluated in the presence of four different natural oils (castor, sunflower, olive and soybean) as well as two different aqueous phases (pure water and phosphate-buffered saline). The results highlighted their interest as surfactant in O/W nanoemulsions for all tested oil and aqueous phases, using a low-energy preparation protocol and relatively low surfactant concentrations. Furthermore, the mannose groups present on the polar head of the surfactant and adsorbed on the surface of the emulsion droplets were shown to retain their native biological properties. The specific mannose-concanavalin A binding was observed *in*

vitro by the designed nanoemulsions, revealing the biorecognition properties of the surfactant and its potential applicability as a nanocarrier.

Keywords: nanoemulsion, biorecognition, mannose, concanavalin A, particle size distribution

1. Introduction

Nanoemulsions are emulsions in the submicrometer range which can be described as a kinetically stable single-phase system with a droplet diameter in the 100 to 500 nm range[1–3]. In this kind of systems, the interface between two immiscible liquids is stabilized by the addition of a surface-active compound in low concentration, *e.g.* a surfactant. This results in a colloidal dispersion where the nature of the components will be directly related to the final properties of the system[4]. A wide range of emulsification methods can be used to produce different types of emulsions, including oil-in-water (O/W), water-in-oil (W/O), or even more complex multiple emulsions, *e.g.* oil-in-water-in-oil (O/W/O) and water-in-oil-in-water (W/O/W) systems[5–7]. Extreme emulsification, phase inversion, nanofluidics, membrane emulsification or satellite droplets are only a few of the most extended methods used in their preparation[8]. With a stability from weeks to months, nanoemulsions are absent of any thermodynamic restrictions or specific temperature effects[9] that can limit their composition, in contrast to microemulsions, widening their use in drug delivery systems, food, cosmetics, templates or material synthesis[10]. However, new formulations that improve their properties as well as their ecological nature are on demand while maintaining a desired functionality and well-controlled physical properties[11]. Most of the currently in use emulsifiers have a petrochemical origin. Over the last few years, there is a gradual tendency in their substitution by biomolecules due to the petroleum feedstock decrease and its effect in the climate change[12]. Among all the possible replacements, sugar-based surfactants have emerged as a commercially consistent alternative[13], particularly the ones based on monosaccharides acting as hydrophilic unit. Although they can be obtained from renewable raw materials, they add innate properties such as biodegradability, low toxicity and biocompatibility, thus meeting the principles of green

chemistry[14]. Out of all sugars, D-mannose is one of the most widely used in the food and biomedical fields[15]. Its properties allow it to be used as a novel transgene adjuvant to control chronic neuropathic pain[16], to reduce the risk of urinary tract infections[17], and more importantly, it can be used as an anchor point due to its specific recognition process with mannose-binding lectins (MBLs)[18]. Lectins are a promising tool for the detection of biomarkers, as bacteria or cancer cells, in bodily fluids and tissues[19]. Synthetic mannosylated systems have been recently synthesized[20] and used as vehicles to specifically deliver drugs or antigens to these cells, mostly in the form of vaccines[21,22]. Nevertheless, due to their multivalency, MBLs bind to high-order glycan structures while their affinity for monosaccharides units remains fairly low[23]. Monovalent mannose-based ligands, while able to yield good interactions with mannose receptors, lack the high affinities that multivalent ligands have, in agreement with the cluster effect that leads to more efficient targeting effects[24]. The design of synthetic ligands capable of recognizing glycoreceptors with high affinity and their incorporation to our daily uses is of vital importance.

In the present work, we report the development and applicability of an ecofriendly amphiphile characterized by a mannose-based polar head group and oleic acid tail as nonpolar moiety, (PMan)₉-b-OI, as emulsifier. The branched polysaccharidic head of this surfactant was designed to improve its affinity to MBLs, while maintaining the innate features of the sugar while forming O/W nanoemulsions with vegetable oils. By dynamic light scattering, laser scanning confocal microscopy and turbidity experiments, the emulsion droplets and their stability were characterized. Furthermore, its applicability and biocompatibility properties were elucidated when selectively binding *in vitro* to concanavalin A, a MBL, showing the feasible use of this novel surfactant in the design of biological drug delivery systems, working as nanocarrier.

2. Materials and Methods

2.1. Materials. (PMan)₉-b-OI surfactant (Propargyl-(oligo)-mannopyranoside-b-oleic-acid, mannose, Degree of Polymerization, $\overline{DP} = 9$) was synthesized by our group. Olive oil (from *olivae oleum virginale*, >99%), castor oil (from *ricinus communis*, >99%) and sunflower seed oil (from *helianthus annuus*, >99%) were supplied from Sigma-Aldrich (St. Louis, MO, United States of America). Soybean oil (from *glycine max*, >99%) was purchased from Alfa Aesar (Havervill, MA, United States of America). Phosphate-buffered saline (PBS) 10x solution was obtained from Euromedex (Souffelweyersheim, France). CaCl₂ and MnCl₂·4H₂O salts were supplied by Sigma-Aldrich (St. Louis, MO, United States of America) and Alfa Aesar (Havervill, MA, United States of America), respectively. Nile Red dye, Concanavalin A (ConA, from *canavalia ensiformis*) and Ricinus Communis Agglutinin I (RCA₁₂₀, from castor bean) lectins were purchased from Sigma-Aldrich (St. Louis, MO, United States of America). Ultrapure deionized water, used for cleaning and dispersion preparation, was obtained by a Millipore Milli-Q unit, and pretreated by a Millipore reverse osmosis system (>18.2MΩ cm⁻¹).

2.2. Nanoemulsion preparation. Nanoemulsions were prepared by the weight (with a ± 0.1 mg precision) of the different compounds that form it. (PMan)₉-b-OI was used as surfactant. Castor, soybean, sunflower, and olive oils were employed separately as oleic phases. Ultrapure deionized water as well as phosphate-buffered saline (PBS) (with 0.1 mM CaCl₂ and 0.1 mM MnCl₂, pH = 7.2) were used as aqueous phases. Thus, every nanoemulsion prepared is described in function of its amount of surfactant, water phase and oil phase used (expressed in wt%). The ratio between the compounds in each sample can be obtained from the respective ternary pseudo-phase diagram ((PMan)₉-b-OI/Oil phase/Aqueous phase).

The protocol of preparation was as follows: first, the required amount of (PMan)₉-b-OI was weighed and poured into a vial. Then, the aqueous phase was weighted and added, and the mixture was homogenized for 30 min using a magnetic stirrer (1000 rpm). Finally, oleic phase was also incorporated to the vial, leading to the final desired composition. The final ternary mixture was

homogenized for 24 h using a magnetic stirrer (1400 rpm) at room temperature (*e.g.*, a (PMan)₉-b-OI/Soybean oil/PBS emulsion in a 5/25/70 wt% ratio was made by the stirring at 1000 rpm of 50 mg of surfactant in 700 mg of a PBS solution. Then, 250 mg of soybean oil were added and the final mixture stirred at 1400 rpm for 24h). It is worth noting that specific stirring conditions, time, and speed motion during the preparation of the nanoemulsions were not required to obtain the final dispersions.

2.3. Determination of the Nanoemulsion Region. The boundary of the nanoemulsion region was analyzed at room (25 °C) and human physiological (37 °C) temperatures for the determination of the pseudo-ternary phase diagram. Every diagram corresponds to a cut of the whole ternary phase diagram at constant temperature and pressure, where the amount of (PMan)₉-b-OI used varies between 1 and 5 wt%. The nanoemulsion regions were identified as those dispersions where a final homogeneous and stable one phase system was obtained during at least 14 days.

2.4. Sample preparation protocol for emulsion-lectin recognition studies *in vitro*. A 5/25/70 wt% (PMan)₉-b-OI/Soybean oil/PBS nanoemulsion at 37 °C was diluted in PBS in a 1:1000 ratio. For the DLS measurements, 200 µL of the diluted emulsion in PBS were taken out and 5 µl of a lectin (1 mg/ml in PBS) solution were added in an Eppendorf tube. The mixture was shaken at room temperature for 20 minutes before the lectin was incubated for 40 min at 37 °C under shaking. Finally, solutions were centrifuged at 37 °C for 20 min at 10,000 g. The supernatant was removed, and the residue redispersed in PBS buffer solution prior sample characterization. This washing step was repeated three times before the samples were measured by DLS. For LSCM measurements, the emulsions were loaded with Nile Red as follow : 200 µl of the diluted emulsion were loaded using 20 µl of a 1 mg/mL Nile Red solution in methanol by magnetically stirring the mixture (750 rpm) for 30 min at room temperature. For turbidity measurements, 300 µL of a 0.016 mg/ml solution of the studied lectin (conA or RCA₁₂₀) were added together with 200 µL diluted emulsion into a quartz cuvette and placed in a UV spectrometer.

2.5. Dynamic light scattering. DLS measurements were performed using two different setups depending on the concentration, transparency, and turbidity of the sample. Emulsions were characterized by a Vasco Particle Size Analyzer (Cordouan Technologies, Pessac, France) at 25 °C and 37 °C using a diode laser (wavelength, $\lambda = 532$ nm) and a scattering angle $\theta = 135^\circ$. Based on enhanced DLS, turbid as well as opaque samples can be properly measured and characterized. Diluted samples were studied by a Zetasizer Nano ZS (Malvern Instruments Ltd., United Kingdom) at 25 °C and 37 °C using a He–Ne laser (wavelength, $\lambda = 632$ nm) in a quasi-backscattering angle $\theta = 173^\circ$. In DLS experiments, it can be obtained the normalized intensity or second-order autocorrelation function, $g^{(2)}(q,t)$, which is directly related to the field or first-order autocorrelation function, $g^{(1)}(q,t)$, equation (1), where β is the optical factor with a value close to 1 [25]. In the case of a monodisperse sample describing a Brownian motion, $g^{(2)}(q,t)$ can be defined in function of a single exponential decay. In this case, the diffusion coefficient can be related to the inverse of the decay time, equation (2), being $q = (4\pi n/\lambda) \sin(\theta/2)$ and n the continuous phase refractive index ($n = 1.33$). In Newtonian conditions, spherical particles, and their apparent hydrodynamic diameter, d_{app}^H , can be obtained by the Stokes–Einstein relationship, equation (3), where k_B denotes the Boltzmann constant, T the temperature, and η is the viscosity.

$$g^{(2)}(q, t) - 1 = \beta |g^{(1)}(q, t)|^2 \quad (1)$$

$$D_{app} = 1/\tau q^2 \quad (2)$$

$$d_H^{app} = k_B T / 3\pi\eta D_{app} \quad (3)$$

2.6. UV-Vis spectroscopy. Turbidity experiments were carried out by a Cary 100 UV-Visible (Agilent Technologies, Santa Clara, CA, United States of America) at a fixed wavelength of 420 nm. The dispersions were placed in a 0.5 mL and 10 mm path length quartz cuvette. Their absorbance evolution was followed in a time period of 60 min with a time step of 30 seconds. All protein aggregates scatter light in the visible wavelength region (400 - 700 nm) since their size ranges from nanometer to micrometer [26,27]. Turbidity experiments describe the attenuation of an

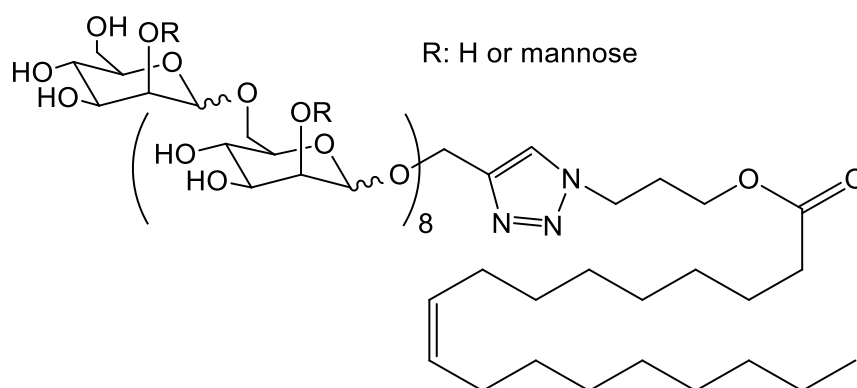
incident beam by light scattering in time due to protein aggregation reactions taking place. Thus, the emulsion-lectin interactions can be tracked.

2.7. Laser scanning confocal microscopy. LSCM images were acquired on an inverted Leica TCS SP5 microscope equipped with a PL APO 0.4 10x air objective (Leica Camera, Wetzlar, Germany). 20 μ L samples were deposited on a planar glass substrate and covered in order to form a thin film prior analysis. The laser outputs were controlled via an Acousto-Optical Tunable Filter (AOTF) and the two collection windows using the Acousto-Optical Beam Splitter (AOBS) and photomultipliers (PMT) as follows: Nile Red was excited with a DPPS diode at 561 nm (15 %) and measured with emission setting at 565 - 600 nm. Aggregates were excited with a He-Ne laser at 633 nm (10 %) in transmission mode. Images were collected using the microscope in sequential mode with a line average of 16.

3. Results and discussion

The main objective of this study was to characterize the emulsifying and biological recognition properties of an engineered sugar-based surfactant. The molecular structure of the amphiphile is based on a mannose oligosaccharide polar head group linked to a hydrophobic oleic acid tail by “click chemistry”, **Figure 1**. The synthesis procedure and characterization of the mannanolipid, denoted as (PMan)₉-*b*-OI, is described in **SI.1**. A comprehensive overview of the synthesis procedure of similar sugar-based amphiphiles has already been reported[28]. In brief, the surfactant is described as having a mannose-based polar head group with a high average degree of polymerization, $\overline{DP} = 9$, and a dispersity, $\overline{D} = 2$, as expected for a polycondensation synthesis. Most of the monosaccharide units are linearly connected via α -(1,6)-linkages along with a partial presence of α -(1,2)-linkages, leading to its final branched pattern. Thus, the polar head group, (PMan)₉, can be depicted as a long sugar-based branched moiety with free D-(+)-Mannose terminal sugars. The final nonionic surfactant is characterized as a mainly hydrophilic molecule, with a theoretical

167 average hydrophilic-lipophilic balance, HLB, of 15, which tends to form oil-in-water (O/W)
168 emulsions[29].



169

170 **Figure 1.** Molecular structure of the mannolipid. R denotes the α -(1,2) mannose ramification
171 position.

172

173 3.1. Determination and characterization of the nanoemulsion region.

174 A preliminary step, in connection with the use of O/W nanoemulsions as active carriers, is the
175 determination of the composition range in which nanoemulsions are formed. As starting point, the
176 nanoemulsions were studied under simplified conditions to further determine the effects of PBS and
177 temperature on the system. Using a pseudo-ternary phase diagram, different (PMan)_{9-b}-
178 OI/Oil/Water ratios were tested at a fixed temperature of 25°C. A set of different vegetable oils
179 (castor, sunflower, olive, and soybean) with similar nature to the hydrophobic region of the
180 surfactant were studied in order to increase the stability of the emulsion.[25] Emulsions based on
181 vegetable oils are easily accessible and biocompatible with and extended use in our daily uses.
182 Castor oil as oil phase is used to obtain oil-in-water nanoemulsions capable of successfully
183 solubilizing quercetin, a natural polyphenol occurring in anti-inflammatory, antibacterial,
184 antioxidant, antiangiogenic, and antitumor activities,[26] while sunflower seed oil is used to
185 encapsulate of both hydrophilic (i.e., iron oxide nanoparticles) and lipophilic (i.e., rhodamine B or
186 epirubicin) materials.[26] Considering the applicability of the emulsion, the pseudo-ternary phase
187 diagram was a cutoff of the true phase diagram containing a maximum concentration of (PMan)_{9-b}-

b -OI, c_s , of 5 wt%. Compared to microemulsions, low c_s are used in nanoemulsions to reduce their toxicity[30]. In addition, the total concentration of the oil phase, c_o , was considered to be in the range of 0 – 45 wt%. Beyond this concentration, the oil would be the main phase present in the system, which would make impossible the use of the O/W nanoemulsion term.

In all (PMan)₉- b -OI/Oil/Water systems tested, nanoemulsions were obtained when the surfactant and oil concentrations ranged between 0.5–5 and 1–25 wt%, respectively. While stable nanoemulsions were obtained at all tested c_s , at c_o above 25 wt%, most of the dispersions were unstable. They were characterized by a clear phase separation in which the two main liquid constituent components used, aqueous and oleic, split after a creaming process. **Figure 2** shows characteristics photos of the samples and the ternary phase diagram of (PMan)₉- b -OI/Castor oil/Water, as example. As it can be seen, although stable in the c_s range of 1 to 5 wt%, no turbidity changes are observed when the c_o is varied up to 25 wt%, maintaining its milky appearance.

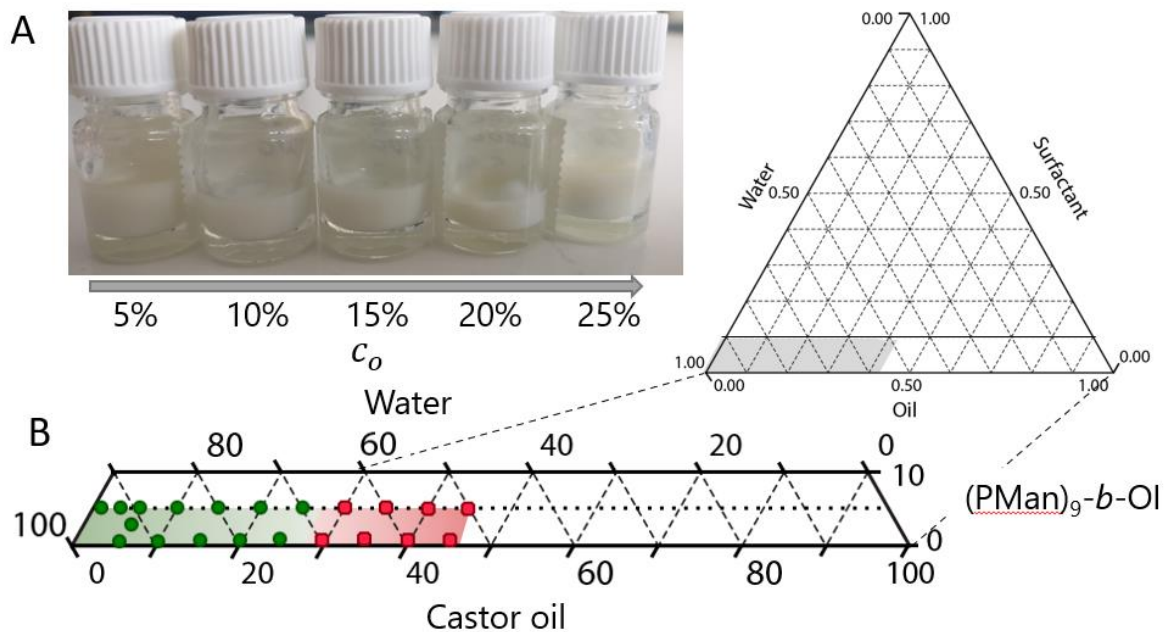


Figure 2. (a) Photos of the dispersions of (PMan)₉- b -OI/Castor oil/Water emulsions increasing the castor oil ratio from left to right at a fixed 5 wt% of surfactant. (b) Ternary phase diagram representing a cut of the whole phase wt% diagram obtained at 25°C for the (PMan)₉- b -OI/Castor oil/Water system. Studied oil-in-water (O/W) nanoemulsion region is evidenced in gray. Stable and

unstable O/W nanoemulsions are denoted by green and red dots, respectively. Notice that the axes represent the wt% of every component.

Moreover, similar results were obtained for other dispersed phases, such as sunflower, olive, and soybean oils. **SI.2** shows the photos and the ternary phase diagrams of each oil with each sample composition tested. The stability of the nanoemulsions can be related to the chemical structure of these natural oils, based on different ratios of ricinoleic, palmitic, oleic, linoleic and linolenic acid, in line with the hydrophobic tail of the surfactant. (PMan)₉-*b*-OI, as a nonionic surfactant, mainly promotes the stabilization by steric repulsions, limiting the molecular approach to the fluid interface. The mannose-based polar head is faced to the continuous aqueous media while the hydrophobic oleic-based tail does it to the oleic one. In this way, the surfactant is positioned as a steric barrier, reducing the surface tension and increasing its elasticity, preventing fluctuations that could lead to coalescence processes. While a bulky hydrophilic moiety is relevant as a steric barrier, as in (PMan)₉, so is the structure of the hydrophobic one. A difference in the chemical structure of the lipophilic tail respect to the oil clearly affects the stabilization of the nanoemulsion. Consequently, mineral oil, characterized by saturated and aromatic structures, led to phase separation, **SI.2**.

While in an aqueous media surfactants with similar molecular structure self-assemble into micelles with mean hydrodynamic diameter values, d_H^{app} , of *c.a.* 10 nm,[31] when used in an emulsified system, (PMan)₉-*b*-OI form droplets characterized d_H^{app} of *ca.* 160 to 350 nm, depending on the oil and surfactant concentrations. All the O/W nanoemulsions denoted an average PDI of *ca.* 0.2 and a minimum stability of 14 days at room temperature, as indicated by DLS. **SI.3** collects each d_H^{app} value over time for each sample. As expected, a direct relationship between the oil:water and surfactant:oil ratios was observed in the final size of the nanoemulsion. At a constant (PMan)₉-*b*-OI c_s of 1 wt%, an increase in the oil:water ratio leads to higher d_H^{app} values, **Figure 3a**. A constant amount of surfactant molecules are available to cover a higher amount of oleic phase. Therefore,

the extra amount of oil must be redistributed in the system, namely inside the droplets, which leads to an increase in droplet size. When this ratio increases and a c_o of 30 wt% is reached, irrespective of the type of oil, the system becomes unstable and the emulsion phase separates. Same d_H^{app} trend was observed for similar oil:water ratios when the c_s was increased to 5 wt%, **Figure 3b**. However, the use of larger amount of surfactant seems to have no effect or slightly increase the d_H^{app} and polydispersity of the droplets. Note that, in the case of simple surfactants, an increase in c_s is associated to a decrease in the average droplet size. A higher surfactant concentration allows the oil droplets to be more dispersed while remaining coated, which reduces the surface tension of the smaller droplets[32]. (PMan)₉-*b*-OI, due to its complex molecular structure and the unique behavior of sugar-derivatives at interfaces, can undergo an assembly reorganization at the interface as function of its concentration. Complex hydrophobic tails have been reported to adopt different configurations depending on the system, such as bent or linear [33,34]. Also, it is known that sugar-sugar hydrogen bonding interactions can also play a key role in the self-assembly processes and the final conformation[35]. Finally, taking into account that non-constant water:oil ratios were used at fixed c_s , it is impossible to accurately compare and explain the effect of the surfactant concentration on the final average size distribution. *E.g.*, 1/25/74 and 5/25/70 wt% (PMan)₉-*b*-OI/Olive oil/Water emulsions are described by 2.96 and 2.8 water:oil ratios, respectively. Nevertheless, as the delimitation of the stable emulsification region was the main objective of the work, further rheological studies are suggested to explain this behavior. Regarding stability, no coalescence was observed after 14 days. A minimal increase in the d_H^{app} and PDI was observed, demonstrating that

the O/W nanoemulsion droplets are quite stable against coalescence, while a phase separation starts to occur after several weeks.

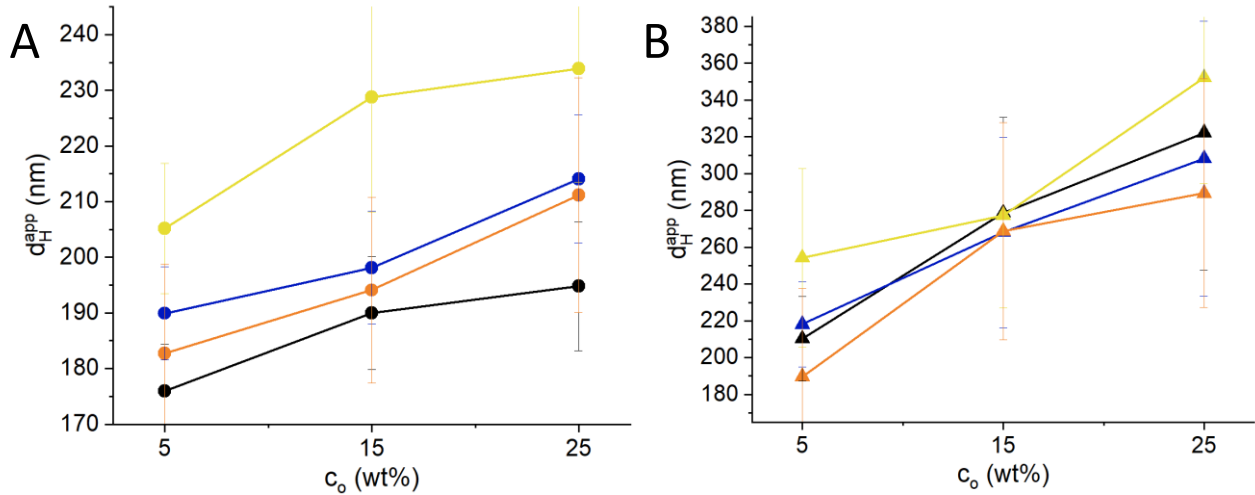
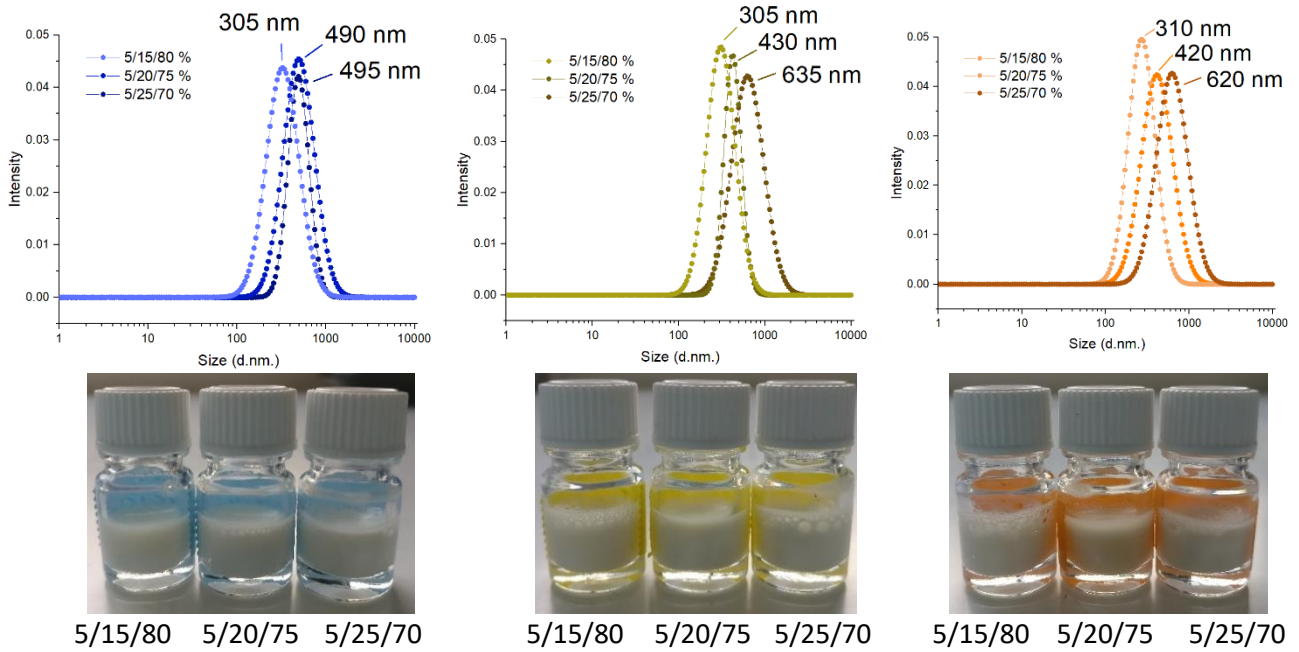


Figure 3. Average droplet size distribution of castor (●,▲), sunflower (●,▲), soybean (●,▲) and olive (●,▲) oil (PMan)₉-b-OI/oil/water nanoemulsions at 25 °C with (a) 1 wt% and (b) 5 wt% c_s .

Considering the applicability of the emulsion, the aqueous medium of the system was replaced by PBS at pH 7.2 and analysed at 37 °C to approximate biological conditions. Nanoemulsions with a c_s of 5 wt% and c_o in the 15 to 25 wt% region were studied, with no visual changes observed in the samples respect their continuous pure water counterparts, denoting their viability in this phosphate-buffered saline medium. Compared to water-based nanoemulsions, the addition of salts to the system and the increase in temperature raised the average droplet size, as shown in **Figure 4**. Although stable, the d_H^{app} values obtained in PBS increased in the c_o 15 to 25 wt% range, compared to MilliQ water-based nanoemulsions, leading to O/W nanoemulsion droplets of *ca.* 200 to 450 nm d_H^{app} . This variation in droplet size is expected. Although the assembly of nonionic surfactants is less affected by ionic strengths and pH changes compared to ionic ones at the time of stabilizing interfaces, changes in the temperature can affect the system stability and surface-tension[36]. It is known that the presence of sodium phosphate increases the surface tension with respect to pure water, destabilizing the interface, promoting the coalescence and therefore the final increase of

268 d_H^{app} . Moreover, a direct relationship between the c_o and d_H^{app} was also observed, as previously in
 269 aqueous media, where an increase of the oil wt%, while decreasing the continuous phase wt%, also
 270 led to a final increase in droplet size.



271 **Figure 4.** Average droplet size distribution of sunflower (●), soybean (●), and olive oil (●)
 272 (PMan)₉-b-OI/oil/PBS nanoemulsions at 37 °C with a c_s 5 wt%.

273

274 3.2. Protein recognition specificity.

275 As a proof of concept, the recognition properties of the nanoemulsion, and specifically of the
 276 designed mannose-based surfactant, were studied under *in vitro* conditions. The behavior of a
 277 1:1000 diluted O/W emulsion of (PMan)₉-b-OI/Soybean oil/PBS (5/25/70 wt%) at 37 °C was
 278 studied after 30 min in the presence of two lectins: Concanavalin A, ConA, and Ricinus Communis
 279 Agglutinin I, RCA₁₂₀. ConA is a lectin known to bind to the monosaccharides D-mannose and D-
 280 glucose [37], whereas RCA₁₂₀ only binds to galactose derivatives[38]. ConA is used as a first *in*
 281 *vitro* test of cellular recognition processes due to its binding properties to various cell membrane
 282 receptors. As a tetravalent ligand, it has four binding sites that, upon activation in the presence of

calcium, can bind up to a total of four D-mannose molecules. By DLS, the multivalent binding of the mannose groups present in the emulsion droplet shell and the ConA can be tracked. In addition, a direct effect of the lectin on the emulsified system could be observed, **Figure 5a**.

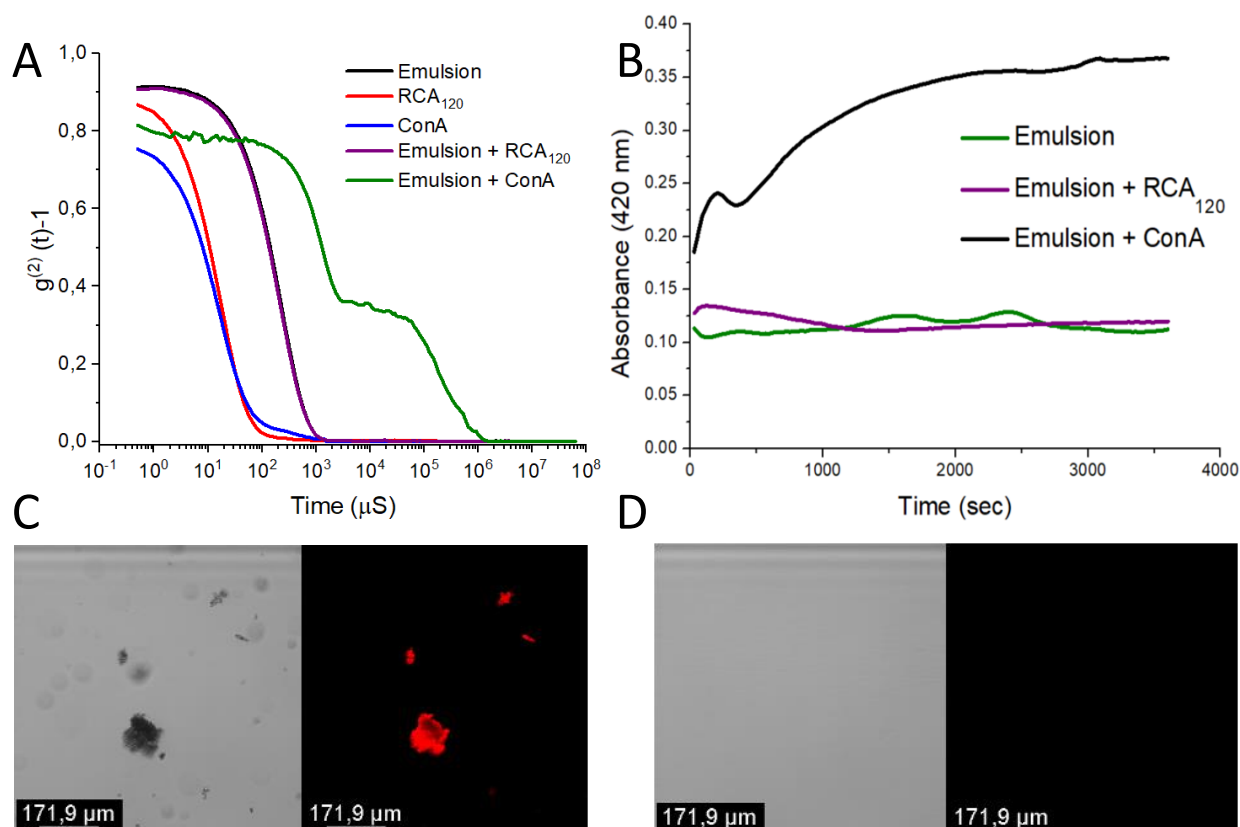


Figure 5. (a) Intensity auto-correlation functions for the (PMan)₉-b-OI/soybean oil/PBS emulsion, lectins and their mixture. (b) Absorbance in time of the (PMan)₉-b-OI/soybean oil/PBS emulsion alone and in presence of the lectins. (c) (PMan)₉-b-OI/soybean oil/PBS emulsion in the presence of ConA and (d) RCA₁₂₀.

While the diluted O/W emulsion of (PMan)₉-b-OI/Soybean oil/PBS denoted a monomodal distribution with a maximum in the 250 nm diameter range, in line with the previous more concentrated samples, a shift to higher times was obtained when ConA was added to the medium. Note that ConA and RCA₁₂₀ are described by an assembly similar to biological conditions, where

297 their shape can be described in form of small individual colloidal particles, as shown by their
298 respective auto-correlation functions[39,40]. In Brownian motion conditions, a longer time
299 corresponds to larger objects or colloids in solution. As expected, the terminal mannose groups of
300 the polar head of the surfactant interact with the lectin, which can also bind to more monosaccharide
301 units due to its multivalency, leading to the formation of random aggregates. Due to this cascading
302 interaction, aggregates were formed on a wide size scale. In contrast, in the presence of RCA₁₂₀ no
303 change in the auto-correlation function was observed with respect to the starting emulsion system,
304 concluding the absence of any interaction between the emulsion droplets and the lectin. To further
305 confirm the specific binding of the (PMan)_{9-b}-OI based emulsion, turbidity experiments were
306 carried out, **Figure 5b**. PBS solutions of each lectin were added to a O/W emulsion of (PMan)_{9-b}-
307 OI/Soybean oil/PBS and their absorbance was measured in time. This method is commonly used
308 for the binding determination between glycosides and lectins[41]. Lectin-emulsion aggregates
309 scatter light in the visible wavelength region, resulting a change of turbidity. Consequently, the
310 formation of aggregates can be directly observed by an increase in light absorbance. As it could be
311 observed, the emulsion in presence of ConA led to their biological recognition and final formation
312 of aggregates, as denoted by the increase in absorbance over time. On the other hand, the presence
313 of RCA₁₂₀ denoted no hallmark of aggregation, characterized by a constant absorbance in time
314 within the error as in the (PMan)_{9-b}-OI/Soybean oil/PBS emulsion alone. Note that the first peak
315 present in the emulsion sample in presence of ConA is related to the experimental set-up. The ConA
316 solution was added on top of the emulsion sample while no stirring and thus no homogenization of
317 the system was applied. A direct view of the final aggregates formed by the mannose-ConA binding
318 process was obtained by LSCM. A 1:1000 diluted 5/25/70 wt% (PMan)_{9-b}-OI/Soybean oil/PBS
319 nanoemulsion was loaded with a lipid-soluble fluorescent dye, Nile Red, which allowed the tracking
320 of the droplets by fluorescence without affecting the d_H^{app} of the emulsion or its stability, **SI.4a**.
321 Consistent with DLS and turbidity results, aggregates were observed in the μm range when the O/W

emulsion was in presence of ConA, **Figure 5c** and **SI.4b**. Note that only focused aggregates could be properly excited and characterized by fluorescence. However, when in the presence of the negative control, RCA₁₂₀, no aggregation-induced effect was observed due to the absence of any mannose-RCA₁₂₀ interaction, **Figure 5d**.

4. Conclusions

We have successfully developed the formulation and application of an environmentally friendly amphiphile based on a mannose oligosaccharide polar head group and a hydrophobic oleic acid tail. At lower concentrations, in the range of 1 to 5 wt%, the designed surfactant forms stable O/W nanoemulsions for at least 14 days. Capable of dispersing natural oils such as castor, sunflower, olive, and soybean up to a 25 wt%, the final emulsion droplets are characterized by hydrodynamic sizes in the *ca.* 160 to 350 nm diameter range, depending on the oil and surfactant concentrations, using water at 25 °C as aqueous media. Under buffer conditions and at 37 °C, the size distribution of the nanoemulsions droplets increases to the *ca.* 200 to 450 nm range, as explained by the temperature increase and the presence of salts that can destabilize the interface and promote droplet coalescence. In addition, the O/W nanoemulsions retained the specific biorecognition nature of the sugar. *In vitro* studies evidence how the mannose residues bind to ConA proteins, a lectin similar to human cellular membrane receptors, as MBL[42]. DLS, turbidity and LSCM experiments denote their interaction and cluster formation. Due to the branching of the surfactant and the multivalency of ConA a cascade binding reaction occurs and aggregates are formed from the emulsion droplets and lectin. The surfactant used in the present work opens a new route to produce biofriendly amphiphiles that could replace chemical surfactants for biological recognition processes and future drug delivery applications, as similar sugar-based surfactants that worked under the same *in vitro* conditions proposed here also did it *in cellulo*.[43] Novel mannose-based surfactants could be synthesized to target alveolar macrophages[40]. Not only focused on D-(+)-Mannose, other sugars

could also be envisioned to target additional receptors. Galactose-based ones could be developed for the recognition of Ricinus Communis Agglutinin, RCA₁₂₀,^[44] while fucose derivatives would bind to Ulex europaeus agglutinin lectin^[45], both with further applications in fungal and herbal environments, respectively.

Associated Content

Supporting Information. MALDI-TOF and ¹H NMR spectra of (PMan)₉. Synthesis protocol and ¹H NMR spectra of (PMan)₉-*b*-OI. Average droplet size and photos of (PMan)₉-*b*-OI/oil phase/aqueous phase systems. Confocal images of ConA recognition experiments. The following files are available free of charge: Supporting_Information (PDF)

Author Information

Corresponding Author

* pgomezargud@enscbp.fr (P. A.)

* Sebastien.Lecommandoux@enscbp.fr (S. L.)

Author Contributions

The manuscript was written through contributions of all authors. All authors have given approval to the final version of the manuscript. ‡These authors contributed equally.

ORCID

Pablo G. Argudo - [0000-0001-5964-727X](https://orcid.org/0000-0001-5964-727X)

Lea Spitzer - [0000-0002-0530-1262](https://orcid.org/0000-0002-0530-1262)

Emmanuel Ibarboure - [0000-0001-8614-3851](https://orcid.org/0000-0001-8614-3851)

368 François Jerome - [0000-0002-8324-0119](https://orcid.org/0000-0002-8324-0119)

369 Henri Cramail - [0000-0001-9798-6352](https://orcid.org/0000-0001-9798-6352)

370 Sébastien Lecommandoux - [0000-0003-0465-8603](https://orcid.org/0000-0003-0465-8603)

371 **Acknowledgment**

372 P.G.A., L.S., E.I., H.C., S.L. acknowledge the Centre National de la Recherche Scientifique, the
373 Région Nouvelle Aquitaine, and the Université de Bordeaux. F.J. is thankful to the Université de
374 Poitiers.

375 **References**

- 376 [1] T. Sheth, S. Seshadri, T. Prileszky, M.E. Helgeson, Multiple nanoemulsions, *Nat. Rev.*
377 *Mater.* 5 (2020) 214–228. <https://doi.org/10.1038/s41578-019-0161-9>.
- 378 [2] J.M. Gutiérrez, C. González, A. Maestro, I. Solè, C.M. Pey, J. Nolla, Nano-emulsions: New
379 applications and optimization of their preparation, *Curr. Opin. Colloid Interface Sci.* 13
380 (2008) 245–251. <https://doi.org/10.1016/j.cocis.2008.01.005>.
- 381 [3] M.M. Fryd, T.G. Mason, Advanced nanoemulsions, *Annu. Rev. Phys. Chem.* 63 (2012)
382 493–518. <https://doi.org/10.1146/annurev-physchem-032210-103436>.
- 383 [4] A. Ostróżka-Cieślik, B. Sarecka-Hujar, The Use of Nanotechnology in Modern
384 Pharmacotherapy, *Multifunct. Syst. Comb. Deliv. Biosensing Diagnostics.* (2017) 139–158.
385 <https://doi.org/10.1016/b978-0-323-52725-5.00007-1>.
- 386 [5] V.K. Rai, N. Mishra, K.S. Yadav, N.P. Yadav, Nanoemulsion as pharmaceutical carrier for
387 dermal and transdermal drug delivery: Formulation development, stability issues, basic
388 considerations and applications, *J. Control. Release.* 270 (2018) 203–225.
389 <https://doi.org/10.1016/j.jconrel.2017.11.049>.
- 390 [6] Z. Zhi, R. Liu, W. Wang, K. Dewettinck, F. Van Bockstaele, Recent progress in oil-in-
391 water-in-oil (O/W/O) double emulsions, *Crit. Rev. Food Sci. Nutr.* (2022) 1–12.
392 <https://doi.org/10.1080/10408398.2022.2029346>.
- 393 [7] I. Kłodová, J. Štětina, Š. Horácková, W/O/W Multiple Emulsions as the Functional

- 394 Component of Dairy Products, *Chem. Eng. Technol.* 42 (2019) 715–727.
395 <https://doi.org/10.1002/ceat.201800586>.
- 396 [8] M.Y. Koroleva, E. V Yurtov, Nanoemulsions: the properties, methods of preparation and
397 promising applications, *Russ. Chem. Rev.* 81 (2012) 21–43.
398 <https://doi.org/10.1070/rc2012v081n01abeh004219>.
- 399 [9] R.B. Patel, M.R. Patel, S.D. Thakore, B.G. Patel, Nanoemulsion as a Valuable
400 Nanostructure Platform for Pharmaceutical Drug Delivery, *Nano- Microscale Drug Deliv.*
401 *Syst. Des. Fabr.* (2017) 321–341. <https://doi.org/10.1016/B978-0-323-52727-9.00017-0>.
- 402 [10] A. Gupta, H.B. Eral, T.A. Hatton, P.S. Doyle, Nanoemulsions: Formation, properties and
403 applications, *Soft Matter*. 12 (2016) 2826–2841. <https://doi.org/10.1039/c5sm02958a>.
- 404 [11] D.G. De Almeida, R. de C.F. Soares Da Silva, J.M. Luna, R.D. Rufino, V.A. Santos, I.M.
405 Banat, L.A. Sarubbo, Biosurfactants: Promising molecules for petroleum biotechnology
406 advances, *Front. Microbiol.* 7 (2016) 1–14. <https://doi.org/10.3389/fmicb.2016.01718>.
- 407 [12] D. Welsby, J. Price, S. Pye, P. Ekins, Unextractable fossil fuels in a 1.5 °C world, *Nature*.
408 597 (2021) 230–234. <https://doi.org/10.1038/s41586-021-03821-8>.
- 409 [13] C.F. Jesus, A.A.S. Alves, S.M. Fiuza, D. Murtinho, F.E. Antunes, Mini-review: Synthetic
410 methods for the production of cationic sugar-based surfactants, *J. Mol. Liq.* 342 (2021)
411 117389. <https://doi.org/10.1016/j.molliq.2021.117389>.
- 412 [14] C.C. Ruiz, *Sugar-Based Surfactants: Fundamentals and Applications*, 1st ed., CRC Press,
413 2008.
- 414 [15] X. Hu, Y. Shi, P. Zhang, M. Miao, T. Zhang, B. Jiang, d-Mannose: Properties, Production,
415 and Applications: An Overview, *Compr. Rev. Food Sci. Food Saf.* 15 (2016) 773–785.
416 <https://doi.org/10.1111/1541-4337.12211>.
- 417 [16] E.C. Dengler, L.A. Alberti, B.N. Bowman, A.A. Kerwin, J.L. Wilkerson, D.R. Moezzi, E.
418 Limanovich, J.A. Wallace, E.D. Milligan, Improvement of spinal non-viral IL-10 gene
419 delivery by D-mannose as a transgene adjuvant to control chronic neuropathic pain, *J.*
420 *Neuroinflammation*. 11 (2014) 1–21. <https://doi.org/10.1186/1742-2094-11-92>.
- 421 [17] R. Milandri, T. Bocchialini, M. Maltagliati, M. Cotugno, E. Simonetti, S. Ferretti, U.V.
422 Maestroni, B.M.C. Rocco, S. Micali, Effects of D-Mannose, ElliroseTM and lactobacillus
423 plantarum in treatment of urinary tract recurrent infections (rUTIs): A survey of urologists

424 knowledge about its clinical application, *Acta Biomed.* 91 (2020) 15–20.
 425 <https://doi.org/10.23750/abm.v91i1.8607>.

426 [18] C. Auriti, G. Prencipe, M. Moriondo, I. Bersani, C. Bertaina, V. Mondì, R. Inglese,
 427 Mannose-Binding Lectin: Biologic Characteristics and Role in the Susceptibility to
 428 Infections and Ischemia-Reperfusion Related Injury in Critically Ill Neonates, *J. Immunol.*
 429 *Res.* 2017 (2017). <https://doi.org/10.1155/2017/7045630>.

430 [19] O.H. Hashim, J.J. Jayapalan, C.S. Lee, Lectins: An effective tool for screening of potential
 431 cancer biomarkers, *PeerJ.* 2017 (2017) 1–30. <https://doi.org/10.7717/peerj.3784>.

432 [20] S. Cecioni, A. Imberty, S. Vidal, Glycomimetics versus multivalent glycoconjugates for the
 433 design of high affinity lectin ligands, *Chem. Rev.* 115 (2015) 525–561.
 434 <https://doi.org/10.1021/cr500303t>.

435 [21] N. Kojima, L. Biao, T. Nakayama, M. Ishii, Y. Ikehara, K. Tsujimura, Oligomannose-
 436 coated liposomes as a therapeutic antigen-delivery and an adjuvant vehicle for induction of
 437 in vivo tumor immunity, *J. Control. Release.* 129 (2008) 26–32.
 438 <https://doi.org/10.1016/j.jconrel.2008.03.023>.

439 [22] M.J. Copland, M.A. Baird, T. Rades, J.L. McKenzie, B. Becker, F. Reck, P.C. Tyler, N.M.
 440 Davies, Liposomal delivery of antigen to human dendritic cells, *Vaccine.* 21 (2003) 883–
 441 890. [https://doi.org/10.1016/S0264-410X\(02\)00536-4](https://doi.org/10.1016/S0264-410X(02)00536-4).

442 [23] C.P. Swaminathan, N. Surolia, A. Surolia, Role of water in the specific binding of mannose
 443 and manno oligosaccharides to concanavalin A, *J. Am. Chem. Soc.* 120 (1998) 5153–5159.
 444 <https://doi.org/10.1021/ja9733696>.

445 [24] S. Espuelas, C. Thumann, B. Heurtault, F. Schuber, B. Frisch, Influence of ligand valency
 446 on the targeting of immature human dendritic cells by mannosylated liposomes, *Bioconjug.*
 447 *Chem.* 19 (2008) 2385–2393. <https://doi.org/10.1021/bc8002524>.

448 [25] B.J.. Berne, R. Pecora, *Dynamic Light Scattering with Applications to Chemistry, Biology,*
 449 *and Physics*, Inc., Pub, New York, USA, 2003.
 450 <https://doi.org/https://doi.org/10.1021/ed054pA430.1>.

451 [26] C.F. Bohren, D.R. Huffman, *Absorption and Scattering of Light by Small Particles*, Wiley,
 452 1998. <https://doi.org/10.1002/9783527618156>.

453 [27] M. Elimelech, J. Gregory, X. Jia, R.A. Williams, *Particle Deposition & Aggregation*,

- Elsevier, 1995. <https://doi.org/10.1016/B978-0-7506-7024-1.X5000-6>.
- [28] L. Spitzer, S. Lecommandoux, H. Cramail, F. Jérôme, Sequential acid-catalyzed alkyl glycosylation and oligomerization of unprotected carbohydrates, *Green Chem.* 23 (2021) 1361–1369. <https://doi.org/10.1039/d0gc04198j>.
- [29] H.T. Davis, Factors determining emulsion type: Hydrophile-lipophile balance and beyond, *Colloids Surfaces A Physicochem. Eng. Asp.* 91 (1994) 9–24. [https://doi.org/10.1016/0927-7757\(94\)02929-6](https://doi.org/10.1016/0927-7757(94)02929-6).
- [30] D.J. McClements, Advances in edible nanoemulsions: Digestion, bioavailability, and potential toxicity, *Prog. Lipid Res.* 81 (2021) 101081. <https://doi.org/10.1016/j.plipres.2020.101081>.
- [31] P.G. Argudo, L. Spitzer, F. Jerome, H. Cramail, L. Camacho, S. Lecommandoux, Design and Self-Assembly of Sugar-Based Amphiphiles: Spherical to Cylindrical Micelles, *Langmuir.* (2022). <https://doi.org/10.1021/acs.langmuir.2c00579>.
- [32] L. Fernández-Peña, S. Gutiérrez-Muro, E. Guzmán, A. Lucia, F. Ortega, R.G. Rubio, Oil-in-water microemulsions for thymol solubilization, *Colloids and Interfaces.* 3 (2019). <https://doi.org/10.3390/colloids3040064>.
- [33] M.K. Nagarajan, J.P. Shah, Conformation and phase transitions in monolayers of some C18 fatty acids containing a hydratable functional group in their alkyl chains, *J. Colloid Interface Sci.* 80 (1981) 7–19. [https://doi.org/10.1016/0021-9797\(81\)90154-5](https://doi.org/10.1016/0021-9797(81)90154-5).
- [34] A. Bhadani, K. Iwabata, K. Sakai, S. Koura, H. Sakai, M. Abe, Sustainable oleic and stearic acid based biodegradable surfactants, *RSC Adv.* 7 (2017) 10433–10442. <https://doi.org/10.1039/C6RA27036K>.
- [35] T. Gaudin, H. Lu, G. Fayet, A. Berthault-Drelich, P. Rotureau, G. Pourceau, A. Wadouachi, E. Van Hecke, A. Nesterenko, I. Pezron, Impact of the chemical structure on amphiphilic properties of sugar-based surfactants: A literature overview, *Adv. Colloid Interface Sci.* 270 (2019) 87–100. <https://doi.org/10.1016/j.cis.2019.06.003>.
- [36] D.J. McClements, *Food Emulsions*, CRC Press, 2004. <https://doi.org/10.1201/9781420039436>.
- [37] D. Diwan, K. Shinkai, T. Tetsuka, B. Cao, H. Arai, T. Koyama, K. Hatano, K. Matsuoka, Synthetic assembly of mannose moieties using polymer chemistry and the biological

evaluation of its interaction towards concanavalin a, *Molecules*. 22 (2017).
<https://doi.org/10.3390/molecules22010157>.

[38] Z. Ma, Y.G. Jia, X.X. Zhu, Glycopolymers Bearing Galactose and Betulin: Synthesis, Encapsulation, and Lectin Recognition, *Biomacromolecules*. 18 (2017) 3812–3818.
<https://doi.org/10.1021/acs.biomac.7b01106>.

[39] L.M.B. Anaya, R. Petitdemange, M. Rosselin, E. Ibarboure, B. Garbay, E. Garanger, T.J. Deming, S. Lecommandoux, Design of Thermoresponsive Elastin-Like Glycopolypeptides for Selective Lectin Binding and Sorting, *Biomacromolecules*. 22 (2021) 76–85.
<https://doi.org/10.1021/acs.biomac.0c00374>.

[40] H. Brognaro, S. Falke, C.N. Mudogo, C. Betzel, Multi-step concanavalin a phase separation and early-stage nucleation monitored via dynamic and depolarized light scattering, *Crystals*. 9 (2019). <https://doi.org/10.3390/cryst9120620>.

[41] N. Vinson, Y. Gou, C.R. Becer, D.M. Haddleton, M.I. Gibson, Optimised “click” synthesis of glycopolymers with mono/di- and trisaccharides, *Polym. Chem.* 2 (2011) 107–113.
<https://doi.org/10.1039/c0py00260g>.

[42] W. Wang, S. Tian, X. Jiang, S. Pang, H. Shi, M. Fan, Z. Wang, W. Jiang, W. Hu, X. Xiao, R. Lin, Molecular Imaging of *Ulex Europaeus* Agglutinin in Colorectal Cancer Using Confocal Laser Endomicroscopy (With Video), *Front. Oncol.* 11 (2021) 1–9.
<https://doi.org/10.3389/fonc.2021.792420>.

[43] B. Dumat, L. Montel, L. Pinon, P. Matton, L. Cattiaux, J. Fattaccioli, J.M. Mallet, Mannose-Coated Fluorescent Lipid Microparticles for Specific Cellular Targeting and Internalization via Glycoreceptor-Induced Phagocytosis, *ACS Appl. Bio Mater.* 2 (2019) 5118–5126. <https://doi.org/10.1021/acsabm.9b00793>.

[44] Y. Wang, G. Yu, Z. Han, B. Yang, Y. Hu, X. Zhao, J. Wu, Y. Lv, W. Chai, Specificities of *Ricinus communis* agglutinin 120 interaction with sulfated galactose, *FEBS Lett.* 585 (2011) 3927–3934. <https://doi.org/10.1016/j.febslet.2011.10.035>.

[45] J.R. Jass, L.J. Allison, S.M. Stewart, M.R. Lane, *Ulex europaeus* agglutinin-1 binding in hereditary bowel cancer, *Pathology*. 25 (1993) 114–119.
<https://doi.org/10.3109/00313029309084782>.

514 **Graphical abstract**

